Active Site Rearrangement of the 2-Hydrazinopyridine Adduct in *Escherichia coli* Amine Oxidase to an Azo Copper(II) Chelate Form: A Key Role for Tyrosine 369 in Controlling the Mobility of the TPQ−2HP Adduct†

Minae Mure,*,‡,§ Christian R. Kurtis,|| Doreen E. Brown,⊥ Melanie S. Rogers,⊥ Winston S. Tambyrajah,|| Colin Saysell,|| Carrie M. Wilmot,# Simon E. V. Phillips,|| Peter F. Knowles,|| David M. Dooley,*,⊥ and Michael J. McPherson*,||

Department of Chemistry, The University of Kansas, Lawrence, Kansas 66045, Department of Chemistry, University of California, Berkeley, California 94270, Astbury Centre for Structural Molecular Biology, School of Biochemistry and Molecular Biology, University of Leeds, Leeds LS2 9JT, United Kingdom, Department of Chemistry and Biochemistry, Montana State University, Bozeman, Montana 59717, and Department of Biochemistry, Molecular Biology, and Biophysics, University of Minnesota, Minneapolis, Minnesota 55455

Received September 17, 2004

ABSTRACT: Adduct **I** (λ_{max} at ∼430 nm) formed in the reaction of 2-hydrazinopyridine (2HP) and the TPQ cofactor of wild-type *Escherichia coli* copper amine oxidase (WT-ECAO) is stable at neutral pH, 25 °C, but slowly converts to another spectroscopically distinct species with a λ_{max} at ∼530 nm (adduct **II**) at pH 9.1. The conversion was accelerated either by incubation of the reaction mixture at 60 °C or by increasing the pH (>13). The active site base mutant forms of ECAO (D383N and D383E) showed spectral changes similar to WT when incubated at 60 °C. By contrast, in the Y369F mutant adduct **I** was not stable at pH 7, 25 °C, and gradually converted to adduct **II**, and this rate of conversion was faster at pH 9. To identify the nature of adduct **II**, we have studied the effects of pH and divalent cations on the UV−vis and resonance Raman spectroscopic properties of the model compound of adduct **I** (**2**). Strikingly, it was found that addition of Cu^{2+} to **2** at pH 7 gave a product (**3**) that exhibited almost identical spectroscopic signatures to adduct **II**. The X-ray crystal structure of **3** shows that it is the copper-coordinated form of **2**, where the +2 charge of copper is neutralized by a double deprotonation of **2**. These results led to the proposal that adduct **II** in the enzyme is TPQ−2HP that has migrated onto the active site Cu^{2+}. The X-ray crystal structure of Y369F adduct **II** confirmed this assignment. Resonance Raman and EPR spectroscopy showed that adduct **II** in WT-ECAO is identical to that seen in Y369F. This study clearly demonstrates that the hydrogen-bonding interaction between O4 of TPQ and the conserved Tyr (Y369) is important in controlling the position and orientation of TPQ in the catalytic cycle, including optimal orientation for reactivity with substrate amines.

Copper amine oxidases (CAOs)[1] share a high degree of structural similarity despite low sequence identity (*1*). The active site is located in a large β-sandwich domain containing Cu^{2+} coordinated by three His residues and two waters (W_a and W_e in a distorted square-pyramidal geometry) and the 2,4,5-trihydroxyphenylalanine quinone (TPQ) cofactor. In the structures obtained at 100 K from crystals grown under conditions where CAOs are active (*2*−*4*), the TPQ cofactor is not directly ligated to the Cu^{2+}. In these active site structures, the C5 carbonyl group of TPQ is directed toward the proposed substrate binding pocket, close to the conserved catalytic base (D383 in ECAO) where O2 of TPQ is hydrogen bonded to W_a and O4 of TPQ is hydrogen bonded to the hydroxyl group of a conserved Tyr (Y369 in ECAO) as shown in Figure 1. In structures obtained at room temperature, TPQ is in the active conformation, but the electron density for TPQ suggests some limited mobility (i.e., pivoting) along the C1 and C4 axis (*5*, *6*). Y369 appears to play a key role in anchoring TPQ in the catalytically active conformation via a short hydrogen bond to the C4 oxoanion of TPQ (*2*, *7*−*10*). In the structure of the 2-hydrazinopyridine (2HP) bound form of ECAO adduct **I** (Figure 2A) (*11*), this hydrogen bond is even shorter (2.3 Å) than it is in the resting

† This work was supported by grants from the National Institutes of Health (GM27659 to D.M.D.) and from the Biotechnology and Biological Sciences Research Council (24/B04841, 24/B10432, and 24/B13477 to M.J.M., S.E.V.P., and P.F.K.). Structural studies were supported by the North of England Structural Biology Centre (24/SB11269 to M.J.M.) and the Department of Chemistry, University of Kansas (to M.M.). C.R.K. was supported by a BBSRC studentship.

* To whom correspondence should be addressed. M.M.: e-mail, mmure@ku.edu; tel, 785-864-2901; fax, 785-864-5396. M.J.M.: e-mail, M.J.McPherson@bmb.leeds.ac.uk; tel, +44 113 233-2595; fax, +44 113 233-3167. D.M.D.: e-mail, dmdooley@montana.edu; tel, 406-994-4373; fax, 406-994-7989.

‡ The University of Kansas.

§ University of California, Berkeley.

|| University of Leeds.

⊥ Montana State University.

University of Minnesota.

[1] Abbreviations: AGAO, *Arthrobacter globiformis* amine oxidase; CAOs, copper amine oxidases; ECAO, *Escherichia coli* amine oxidase; EPR, electron paramagnetic resonance; HPAO, *Hansenula polymorpha* amine oxidase; 2HP, 2-hydrazinopyridine; rR, resonance Raman; PSB, product Schiff base; SSB, substrate Schiff base; TPQ, topa quinone (2,4,5-trihydroxyphenylalanine quinone); WT-ECAO, wild-type ECAO.

10.1021/bi0479860 CCC: $30.25
Published on Web 01/11/2005

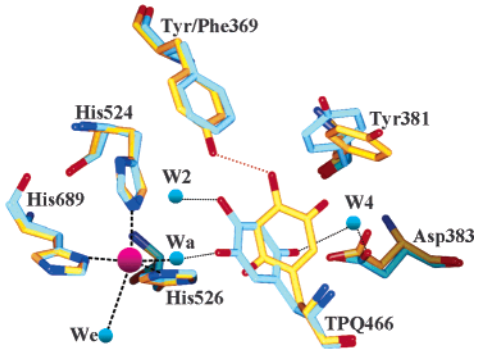

FIGURE 1: Superimposed view of the active sites of WT-ECAO (yellow) and Y369F-ECAO (cyan). Highlighted in red is the key hydrogen-bonding interaction that is present in WT-ECAO but not in Y369F. Water molecule W5 observed in the WT-ECAO structure has been lost to a new water, W4, in the Y369F structure. The copper ion is represented as a magenta sphere, and water molecules are represented as blue spheres.

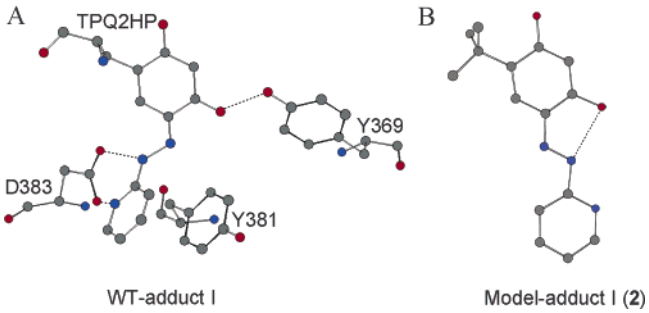

FIGURE 2: Ball and stick representation of the active site of WT-ECAO adduct **I** (A) and **2** (B). Key: gray spheres, carbon; red spheres, oxygen; blue spheres, nitrogen. Dashed lines represent hydrogen-bonding interactions.

form (2.7 Å). It has also been proposed that Y369 is involved in a proton shuttle from the substrate-reduced TPQ cofactor to dioxygen in the catalytic cycle (*7*, *12*).

Mutation of Y369 to eliminate the hydrogen-bonding interaction (Y369F) did not affect K_m for β-phenylethylamine significantly, while k_{cat} is decreased 40-fold (*2*). The X-ray crystal structure of Y369F-ECAO was solved to 2.1 Å resolution at 100 K (Figure 1) (*2*). In the Y369F structure, C5 and O5 of TPQ are well refined and O5 of TPQ is close to W_a. The O2 atom of TPQ in Y369F interacts via a water molecule, W4, with the carboxylate oxygen of the catalytic base, D383. The O4 oxoanion of TPQ makes a hydrogen bond (2.4 Å) with a water molecule, W2, which is found in all reported WT structures of CAOs. Removal of the hydroxyl group of Y369 gives TPQ more flexibility to adopt alternative conformations in the active site (Figure 1) (*2*). In the crystal structure, a majority of TPQ occupies the catalytically inactive conformation. However, the substantial activity of Y369F observed in solution at room temperature and the full complement of TPQ (1.95 TPQ/dimer) suggests that TPQ has the conformational freedom in this mutant to adopt an optimal orientation during turnover (*2*, *6*).

In the preceding paper (*26*), we have shown that adduct **I** formed from the reaction of WT-ECAO and 2HP exists as a tautomeric mixture, where the hydrazone form is favored over the azo form (Scheme 1). The stabilization of the hydrazone tautomer is achieved by hydrogen-bonding interactions between the hydrazone and protonated D383 and between the C4 oxoanion of TPQ and the hydroxyl group of Y369 (Figure 2A). In contrast, the corresponding model compound (**2**, Scheme 2) isolated from the reaction of a TPQ model (**1**) and 2HP exists predominantly as the azo form where a strong intramolecular hydrogen-bonding interaction between the hydroxyl group at C4 and one of the azo nitrogens was observed (Figure 2B). In WT-ECAO, the equilibrium of the hydrazone form and the azo form is controlled by the protonation state of D383 (Scheme 1). A pK_a of 9.7 was determined for D383 in the adduct **I** form, and this value is ca. 4 pH units elevated when compared to that of D383 in the underivatized resting form of the enzyme. In the D383N and D383E mutants, there were no detectable pK_as between pH 6 and pH 10, confirming the assignment of the pK_a in WT adduct **I**.

When hydrogen-bonding interactions between TPQ−2HP and active site residues in adduct **I** are disrupted, either by deprotonation of D383 (pH >9.7) or by denaturation with 8 M urea at pH 7.0, an immediate blue shift in the λ_{max} (10−15 nm) indicative of the conversion of the hydrazone to the azo tautomer is observed. This azo tautomer of adduct **I** is not stable and gradually converts to a new species with a λ_{max} at ∼530 nm (adduct **II**) in an isosbestic manner. In the Y369F mutant, adduct **I** is much less stable than it is in WT and the D383N and D383E mutants, and a slow conversion to the adduct **II** form was observed even in pH 7 solution at room temperature.

Previously, adduct **II** had been proposed to be the azo tautomer of TPQ−2HP where the tautomerism is "catalyzed" via a proton abstraction of the hydrazone tautomer (adduct **I**) by D383 (*13*). This proposal was based on the role of D383 during the catalytic turnover which abstracts a proton from the substrate Schiff base (SSB) intermediate to form the product Schiff base (PSB). Analogies were made between adduct **I** and the SSB and between adduct **II** and the PSB. In the preceding paper (*26*), we have shown that adduct **I** is actually a tautomeric mixture of hydrazone and azo forms where both are monoanions. The only titratable proton in the adduct **I** structure was assigned to D383.

In this paper, we describe the detailed characterization of adduct **II** in both WT and mutant forms of ECAO (Y369F, D383N, and D383E). To identify the nature of adduct **II**, the effect of divalent cations on the UV−vis and rR spectroscopic properties of model compound **2** has been studied. Strikingly, it was found that stoichiometric addition of Cu^{2+} to **2** at pH 7 gave a product that was essentially identical to adduct **II**, leading to the proposal that adduct **II** in the enzyme is the product of the ligation of TPQ−2HP to the active site Cu^{2+}. A model compound for the Cu^{2+}-coordinated form of TPQ−2HP, **3**, has been synthesized and its structure determined, which revealed a novel Cu^{2+} complex with TPQ−2HP. Y369F forms adduct **II** in a facile manner under mild conditions, allowing for its full structural characterization. We present UV−vis, EPR, and rR spectroscopic and X-ray crystallographic structural characterizations of Y369F adduct **II** and of model compound **3**. We confirm that adduct **II** is the fully deprotonated azo form of TPQ−2HP which is ligated to the active site Cu^{2+}. This result supports the proposed role of Y369 in controlling the mobility of TPQ in the active site (*2*, *3*, *7*−*10*). Further, the formation of adduct **II** in this study shows that both SSB

Scheme 1: Formation of Adduct **I** in WT-ECAO

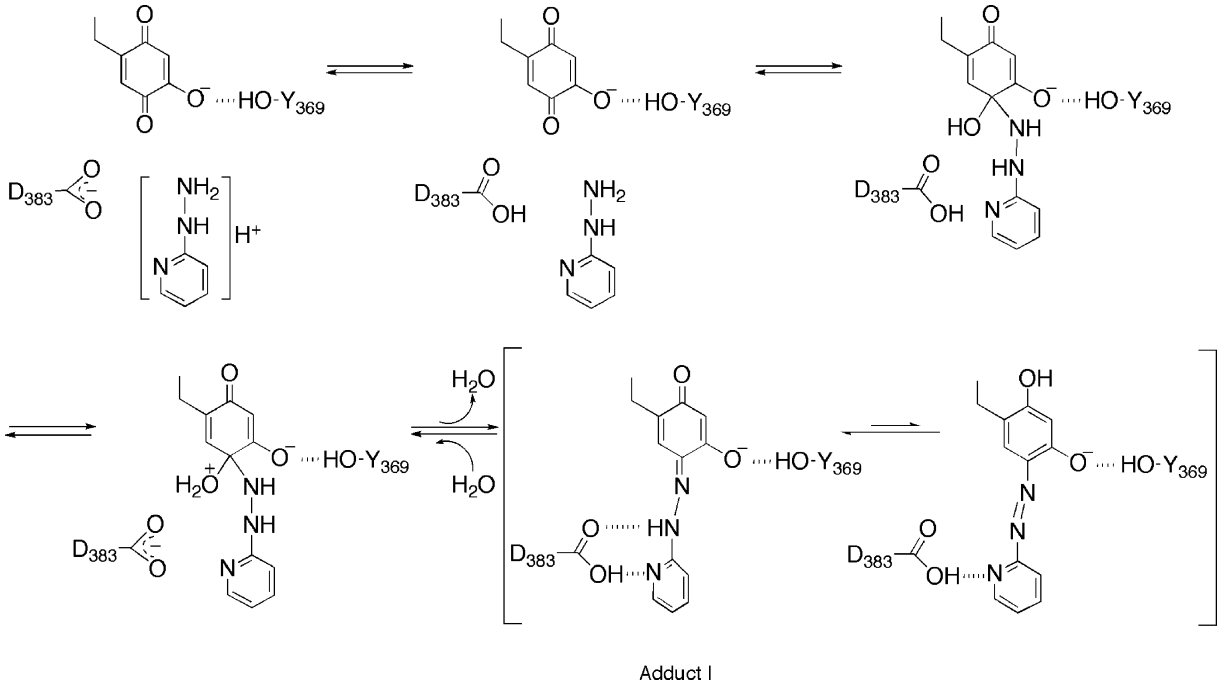

Scheme 2: Formation of **2**

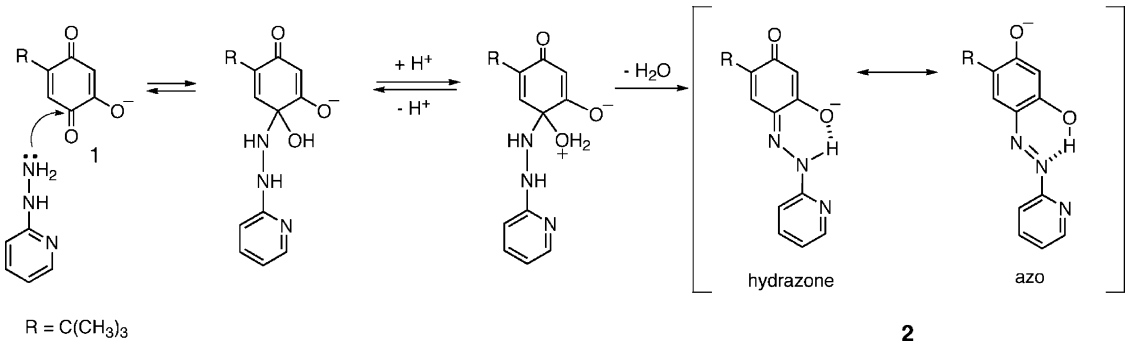

and PSB in the catalytic cycle have the potential for considerable motion within the active site as originally proposed for the active site mutants of HPAO (*9*, *14*−*16*).

EXPERIMENTAL PROCEDURES

Materials. 4-(2-Pyridylazo)-6-*tert*-butylresorcinol (**2**) was prepared as previously described [see preceding paper (*26*)]. Dichloro(1,10-phenanthroline)copper(II), 0.1 M sodium methoxide solution, and anhydrous methanol were purchased from Aldrich and used without further purification.

General. ^{1}H and ^{13}C NMR spectra were obtained on Bruker AM-400 and AM-500 spectrometers. Unless stated otherwise, all UV−vis spectra were obtained on a HP8452A diode array spectrophotometer equipped with a temperature-controlled cell holder.

Protein Purification and Enzyme Assay. WT-ECAO, Y369F, D383E, and D383N were prepared and purified as previously reported (*2*, *8*). The enzyme used in this study was purified to >95% homogeneity as determined by SDS−PAGE. The enzyme concentration was determined from absorbance at 280 nm adjusted by a gravimetrically derived correction factor of 0.76 to give concentration in milligrams per milliliter ($\epsilon = 2.1 \times 10^5$ M^{-1} cm^{-1}) (*13*). All experiments were performed aerobically. Enzyme activity was measured as previously described using a coupled assay with β-phenylethylamine as substrate (*5*).

*Adduct **II** Formation of WT-ECAO.* Formation of adduct **II** in WT-ECAO by thermal conversion was performed by incubating adduct **I** at 60 °C for 30 min or until no further absorbance changes were observed by UV−vis spectroscopy. Sample buffers were 20 mM sodium or potassium phosphate (pH range 6.9−7.2) and 20 mM 2-(*N*-cyclohexylamino)-ethanesulfonic acid (Ches, pH 8−10). All buffers were adjusted with NaCl to give an ionic strength of 0.1 M. Protein concentrations ranged from 2×10^{-6} to 4.5×10^{-6} M. Conversion of adduct **II** at high pH was completed by adding a small aliquot of potassium hydroxide (final concentration 2.85 M, pH ~15) to adduct **I** of WT-ECAO at pH 7.0. Other methods for adduct **II** formation appear elsewhere in the Experimental Procedures.

*Adduct **II** Formation of WT-ECAO, D383E, and D383N by Urea Treatment.* Adduct **I** samples of D393E (0.097 mM) and D393N (0.101 mM) in 0.1 M potassium phosphate, pH 7.2, were prepared by the addition of a 5-fold excess of 2HP. Each derivatized sample (5 μL) was further diluted with 95 μL of 8 M urea prepared in 0.1 M potassium phosphate, pH 7.2, and immediately monitored by UV−vis spectroscopy at room temperature for 30 min. As a control, 110 μL of

WT-ECAO (0.009 mM) was derivatized with 5 μL of 2HP (0.045 mM) and allowed to react for 1 min before the sample was diluted to 600 μL with 8 M urea prepared in 0.1 M potassium phosphate, pH 7.2.

*Adduct **II** Formation of Y369F-ECAO, X-ray Crystallographic Data Collection, and Structure Analysis.* A 1 mL aliquot of 7 mg/mL Y369F ECAO was reacted with 10 molar equiv of 2HP at 37 °C, pH 8.0. The progress of the reaction was followed by scanning UV−vis spectroscopy using a Shimadzu 2401 spectrophotometer. During the first 20 s, the characteristic absorbance of TPQ at ~490 nm was lost, and a highly colored peak at 420 nm formed, corresponding to adduct **I**. Following a further 90 min incubation, the 420 nm absorbance was lost and a new absorbance at 530 nm developed (adduct **II**). After adduct **II** formation was complete, the protein sample was dialyzed against 5000 volumes of 20 mM Tris-HCl (pH 8.0). An aliquot was removed and subjected to electrospray mass spectrometry on a Q-TOF instrument (Micromass U.K. Ltd., Manchester, U.K.) to determine the molecular weight of the 2HP-derivatized protein in comparison with Y369F. The mass increase in the 2HP-derivatized protein was 80 ± 10 amu. The derivatized protein crystals were grown in 1−1.4 M sodium citrate and 20 mM Hepes (pH 6.9−7.3) at 18 °C, using the sitting drop vapor diffusion method. These crystals were transferred to a cryoprotectant solution, containing 15% more sodium citrate than the mother liquor and 20% glycerol, before cooling to 100 K in a cold nitrogen gas stream (Oxford Cryosystems). Diffraction data were collected at the Daresbury SRS (Synchrotron Radiation Source) with a 300 mm MAR CCD detector, at a crystal to detector distance of 200 mm. The protein crystallized in a $P2_12_12_1$ orthorhombic lattice, the same as all other ECAO crystals used for structure determination. The cell dimensions were also typical for ECAO crystals: $a = 135.12$ Å, $b = 167.13$ Å, and $c = 79.64$ Å. Programs from the CCP4 suite (*17*) and DENZO (*18*) were used to process and refine the data. Rigid body refinement was used initially to fit the WT-ECAO model (*8*) into the calculated electron density. The entire molecule was then scanned residue by residue to assess the quality of the fit of the model into the density. The majority of the molecule was rebuilt during this process. Prior to positional and *B*-factor refinement using the CNS suite of programs, the side chains of active site residues Y369, TPQ466, D383, M699, and Y381 and all of the solvent molecules were removed from the model. Following 20 cycles of positional and *B*-factor refinement, $2F_o - F_c$ maps were calculated, and the difference density in the active site was used to systematically replace the residues that had been removed. To refine the structure of the derivatized TPQ moiety, a full dictionary was prepared by adapting files available at http://alpha2.bmc.uu.sc/hicup. Refinement of the TPQ adduct was carried out with no restrictions on the dihedral angles across the TPQ−2HP ring system. This was to allow the rings to adopt any conformation during refinement. Due to the lack of clarity in the electron density in the active site, several models were tested and refined before the final model was accepted as being the majority species. Finally, the positions of ~800 solvent molecules determined using WATPEAK (*17*) were placed in the model and subjected to further positional and *B*-factor refinement. Solvent molecules with a refined *B*-factor of >50 Å^2 were rejected from the final model.

*Effect of Divalent Cations on UV−Vis Absorption Spectra of **2** at Neutral pH.* A 36 μL aliquot of the stock solution ([**2**] = 0.56 mM in 30% methanol−milliQ H_2O) was diluted with 944 μL of a 0.02 M sodium phosphate buffer, pH 7.3 ($\mu = 0.2$ with NaCl), in a quartz cell. A 20 μL aliquot of a stock solution of a divalent metal ion ([M^{2+}] = 10 mM in milliQ H_2O) was added to the cuvette. The spectra were taken immediately after the dilution. Metal salts used were $CuSO_4 \cdot 5H_2O$, $MgSO_4 \cdot 7H_2O$, $CaCl_2 \cdot 2H_2O$, $ZnCl_2$, $NiCl_2 \cdot 6H_2O$, and $CoCl_2 \cdot 6H_2O$.

*UV−Vis Spectroscopic Titration of **2** with Cu^{2+} at Neutral pH.* A 36 μL aliquot of the stock solution ([**2**] = 0.56 mM in 30% methanol−milliQ H_2O) was diluted with 944 μL of a 0.02 M sodium phosphate buffer, pH 7.3 ($\mu = 0.2$ with NaCl), in a quartz cell. The corresponding amount of Cu^{2+} stock solution ([Cu^{2+}] = 1 mM in milliQ H_2O) was added to the solution of **2** to make the final concentration of Cu^{2+} as 2−18 μM. The spectra were taken immediately after the dilution.

*Synthesis of [(Phen)Cu^{II}(**2**)] (**3**).* Compound **2** (100 mg, 0.37 mmol) and a molar equivalent of dichloro(1,10-phenanthroline)copper(II) were suspended in 20 mL of anhydrous methanol. Subsequently, 0.37 mL of 0.1 M sodium methoxide (in methanol solution) was added to the suspension, and the reaction mixture was stirred at room temperature overnight. The solvent was evaporated to dryness, and the resulting mass was dissolved in a minimal amount of hot methanol. The solution remained at room temperature overnight, following which the copper complex (**3**) crystallized as dark green tablets: IR (KBr) 1598 (s), 1502 (m), 1478 (m), 1450 (w), 1378 (s, br), 1310 (w), 1292 (w), 1225 (vs, br), 1187 (vs, br), 1145 (s), 1064 (w), 1014 (w), 965 (w), 888 (w), 859 (w), 821 (w), 777 (w), 742 (w).

*X-ray Crystallographic Structure Determination of **3**.* A fragment of a dark green tablet crystal of **3**, $CuO_6N_5C_{27}H_{24}$, having approximate dimensions of 0.35 × 0.20 × 0.06 mm was mounted on a glass fiber using Paratone N hydrocarbon oil. Diffraction data were collected on a SMART (*19*) CCD with graphite monochromated Mo−Kα radiation. The structure was solved by direct methods (*20*) and expanded using Fourier techniques (*21*). The copper complex was refined anisotropically, while the water oxygens were refined isotropically. Hydrogen atoms were included in the calculated positions but were not refined. All calculations were performed using the teXsan crystallographic software package (Molecular Structure Corp.). Full details of the X-ray structure determination can be found in the Supporting Information.

*Resonance Raman (rR) Spectroscopy of ECAO Adduct **II** and of Model Compounds.* Adduct **I** samples were prepared as described in the preceding paper (*26*). Conversion of adduct **I** to adduct **II** (as monitored by UV−vis spectroscopy) in WT, D383E, and D383N took place by heating the samples (~100 μL) between 35 and 45 °C in an Eppendorf tube for ~1−3 days. For Y369F, conversion from adduct **I** to adduct **II** occurred at room temperature. Protein concentrations ranged from 0.048 to 0.091 mM in 0.1 M potassium phosphate, pH 7.2. Samples of model compound **2** were prepared by addition of a 1:1 stoichiometry of $CuCl_2$ or $CoCl_2$ (prepared in deionized H_2O) to **2** in 0.1 M potassium

phosphate, pH 7.2. A sample of **3** was prepared by adding 1 μL of acetonitrile to a small amount of **3** and then diluting to 1.5 mL with 0.1 M potassium phosphate, pH 7.2. The model at high pH (~11) was prepared by diluting 10 μL of **2** (0.2 mM) to a small amount of 1 M NaOH (<100 μL). rR spectra were collected using a Spex Triplemate spectrophotometer equipped with a liquid nitrogen cooled CCD detector. Excitation at 514.5 nm was provided by a Coherent 400 argon laser. Data were typically collected over 5 min at 40 mW. Raman frequencies were calibrated relative to an aspirin standard, and data analysis was carried out using GRAMS software (Thermo Galactic) and Origin (OriginLab Corp.).

Electron Paramagnetic Resonance Spectroscopy (EPR). EPR data were collected on a Bruker EMX, X-band spectrometer at 77 K. WT-ECAO (0.115 mM) and Y369F (0.0845 mM) samples in 20 mM sodium phosphate, pH 7.2, were prepared by placing ~150 μL of underivatized protein in an EPR tube. A 10-fold excess of 2HP was introduced into the EPR tube by a gastight syringe. Visible absorbance spectra of the sample in the EPR tube were collected before and after the addition of 2HP. Samples turned yellow (adduct **I**) upon mixing and were frozen immediately in liquid nitrogen for data collection. After data collection, samples were thawed. The EPR tube containing WT-ECAO adduct **I** was incubated overnight at 45 °C, leading to the formation of adduct **II**. The conversion of Y369F adduct **I** to adduct **II** was achieved by incubating the sample at 50 °C for 45 min. Samples turned pink upon heating, characteristic of adduct **II** formation. Compound **3** was prepared by dissolving a small amount (~2 mg) of the compound in 150 μL of methanol.

RESULTS

*Conversion of Adduct **I** to Adduct **II** in WT-ECAO.* WT-ECAO adduct **I** is stable at neutral pH, 25 °C. However, incubation of adduct **I** at pH 9.1, 25 °C, led to the slow conversion ($t_{1/2}$ ~ 12 h) to a new species with a λ_{max} at 525 nm (termed adduct **II**) in an isosbestic fashion (isosbestic point at 460 nm) as shown in Figure 3A. The conversion was accelerated by heating the solution to 60 °C and completed within 30 min (Figure 3B). While adduct **I** is stable at room temperature at pH 6.9, incubation at 60 °C for 30 min induces spectral changes similar to those seen at pH 9.1, although the conversion does not go to completion (Figure 3C). A similar 100 nm red-shifted species can also be formed immediately upon room temperature incubation of adduct **I** at high pH (pH >14; Figure 3D). The spectral shift seen in these highly basic conditions is analogous to the "purple shift" observed for the phenylhydrazine and *p*-nitrophenylhydrazine derivatives of TPQ in CAOs (*22*). This high-pH species is likely to be the fully deprotonated form of TPQ−2HP adduct **I** which forms during denaturation of the enzyme, an assignment supported by the pH titration of **2** [see preceding paper (*26*)].

*Conversion of Adduct **I** to Adduct **II** in D383E and D383N.* As in WT-ECAO, adduct **I** in D383N exists as a tautomeric mixture where the hydrazone form is stabilized over the azo form by the hydrogen-bonding interaction between the amide group of N383 and the pyridine nitrogen of the 2HP moiety [see preceding paper (*26*)]. In D383E, the extra methylene in the side chain of Glu compared with Asp helped to

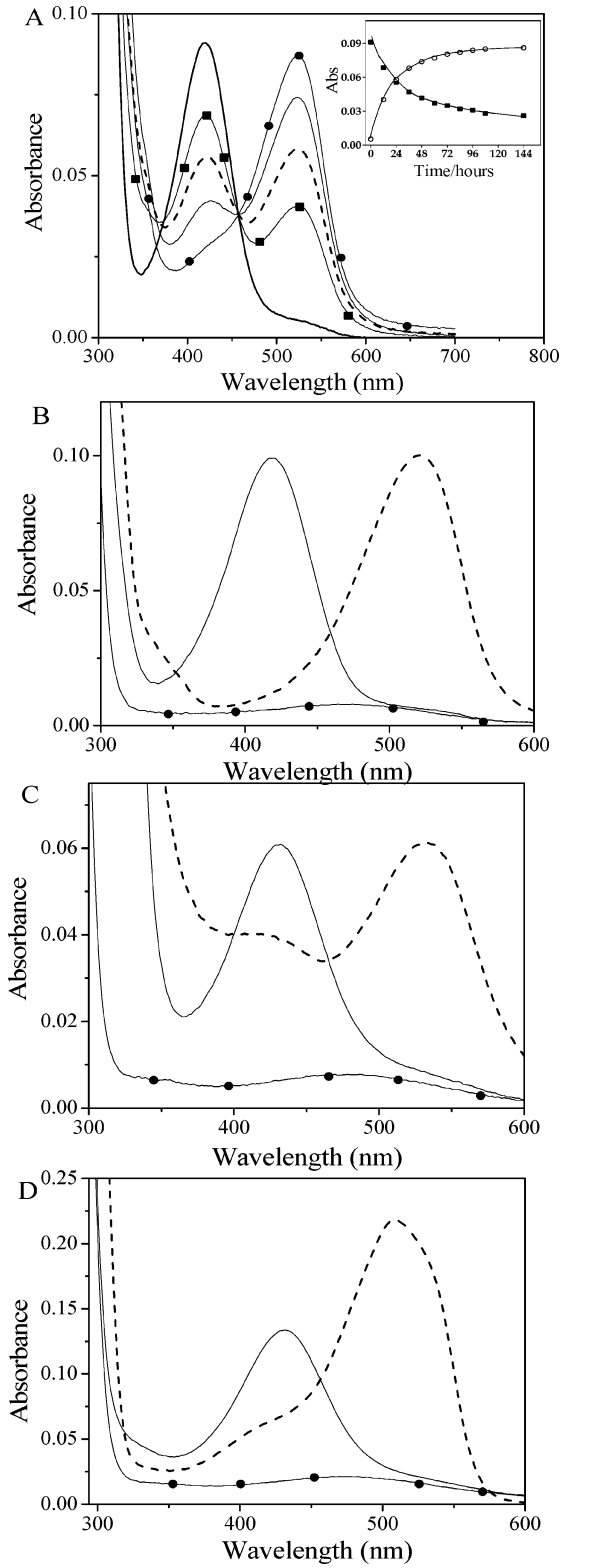

FIGURE 3: (A) UV−vis spectra showing the conversion of adduct **I** to adduct **II** in WT-ECAO (2 μM) in 20 mM Ches, pH 9.1 at 25 °C. Spectral time points: t = 0 (—), t = 12 h (■), t = 24 h (- - -), t = 72 h (−), and t = 120 h (●). [2HP] = 100 μM. The inset shows a plot of the absorbance change of adduct **I** (420 nm, ■) vs adduct **II** (520 nm, ○) over time. (B) UV−vis spectra of the adduct **I** conversion to adduct **II** in WT-ECAO at pH 9.8, 60 °C (C), at pH 6.90, 60 °C, and (D) after the addition of KOH to a final concentration of 2.85 M. Protein concentrations ranged from 2.2 to 4.4 μM. Reactions were initiated by a stoichiometric addition of 2HP. Key: (●) WT-ECAO, (—) adduct **I**, and (- - -) adduct **II**.

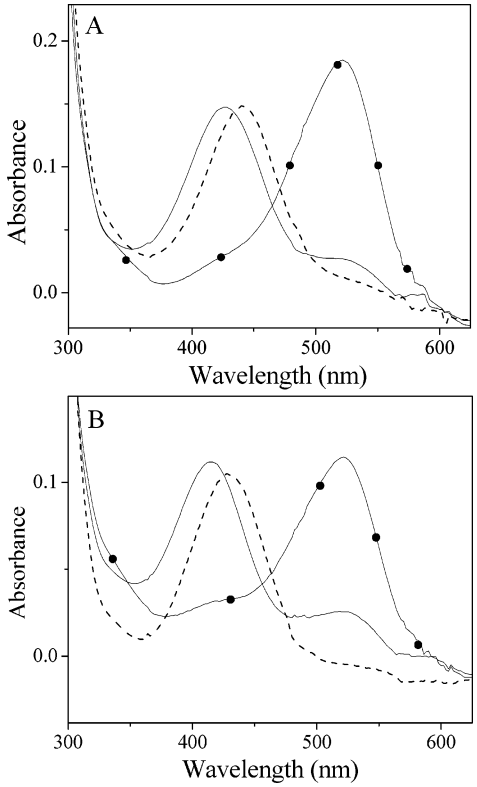

FIGURE 4: UV−vis spectra showing conversion of adduct **I** to adduct **II** in ECAO active site mutants D383E (A) and D383N (B) after the addition of 8 M urea. Key: (- - -) hydrazone form of adduct **I**, (—) azo form of adduct **I**, and (●) adduct **II**. Protein concentrations were 4 and 5 μM, respectively, in 0.1 M potassium phosphate, pH 7.2 at 25 °C.

produce a shorter, stronger hydrogen bond, further shifting the equilibrium of the adduct **I** toward the hydrazone form. In contrast to the observation with WT-ECAO, neither D383E nor D383N adduct **I** forms converted to adduct **II** at pH 9.1 (data not shown). Upon denaturation by 8 M urea at pH 7.2, both D383E and D383N adduct **I** exhibited an immediate blue shift of λ_{max} characteristic of conversion to the azo tautomer, which was not stable and gradually converted to adduct **II** (Figure 4). The spectral changes of WT-ECAO adduct **I** under denaturing conditions were identical to that observed in the D383 mutants (data not shown). This observation is consistent with a common mechanism for adduct **II** formation in the WT and D383 mutants and supports the inference that 8 M urea disrupts the active site hydrogen-bonding interactions in both WT-ECAO and the D383 mutants.

*Conversion of Adduct **I** to Adduct **II** in Y369F-ECAO.* In contrast to the WT and D383 mutants of ECAO, adduct **I** in Y369F is not stable at room temperature, pH 7.0, and undergoes conversion to adduct **II** ($t_{1/2} \sim 3.5$ h; data not shown). At pH 9.0, the conversion is faster and is completed within 90 min (Figure 5). The pH dependency observed most likely reflects the pK_a of D383 [see preceding paper (*26*), p$K_a \sim 9.7$]. The rate of conversion is still faster for Y369F adduct **I** at pH 7.0 than WT adduct **I** at pH 9.1, suggesting that the hydroxyl group of Y369 remains protonated in the latter. Even though D383 is protonated at pH 7.0 and hydrogen bonded to the 2HP moiety in adduct **I**, this is not enough to prevent conversion to adduct **II** in the absence of Y369. These results clearly show that the hydroxyl group

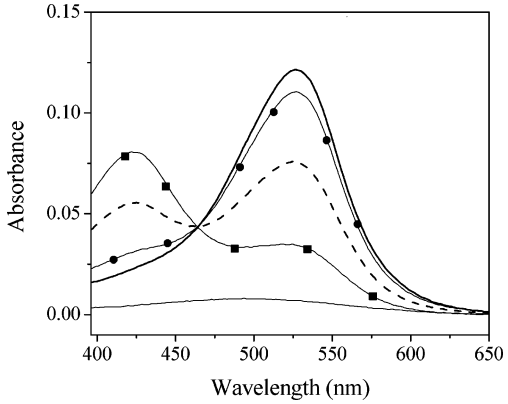

FIGURE 5: UV−vis spectral changes associated with the conversion of adduct **I** to adduct **II** at pH 9.0 in Y369F of ECAO over time. Key: (—) resting form, (■) $t = 2$ min after the addition of 2HP (22 μM), (- - -) $t = 6$ min, (●) $t = 18$ min, and (▬) $t = 90$ min. The protein concentration was 3.2 μM in 20 mM sodium phosphate at 25 °C.

of Y369 plays a prominent role in controlling the conversion of the adduct **I** to adduct **II** and that D383, while involved, has a lesser influence.

*Effect of Divalent Cations on the UV−Vis Spectroscopic Properties of **2** at Neutral pH.* When **2** was treated with an excess (200 molar equiv) of a divalent cation such as Cu^{2+} or Co^{2+} at pH 7.3, the color of the solution changed immediately from yellow to pink. This is reflected in the appearance of an absorption band at 504 nm and a decrease in absorbance at 414 nm (Figure 6A). Ni^{2+} and Zn^{2+} produce similar spectral changes, but the conversion to the species absorbing at 504 nm was not complete. Ca^{2+} and Mg^{2+} (data not shown) did not alter the spectral characteristics of **2** probably due to their preference for oxygen coordination (from solvent water and phosphate) over nitrogen coordination. The λ_{max} of 504 nm is ~10 nm red shifted when compared with that of the species observed at high pH (>13) in the UV−vis spectroscopic titration of **2** [see preceding paper (*26*)]. The binding of **2** to M^{2+} (see below) can lower the pK_a of the 4-hydroxyl group, allowing for deprotonation to occur at neutral pH, indicating that the electronic properties of the metal ion have some influence on the electronic structure of **2**. The small red shift in the λ_{max} around 500 nm as the divalent cation is varied is consistent with this inference.

Because the active site of ECAO contains copper, the effect of Cu^{2+} on the UV−vis spectroscopic properties of **2** was examined. Figure 6B shows the spectral changes observed upon titrating **2** with Cu^{2+}. Figure 6C shows a plot of A_{414} and A_{506} as a function of the **2**:Cu^{2+} molar ratio at pH 7.3. Cu^{2+} binds to **2** forming a 1:1 complex with no further increase in the absorbance at 506 nm observed upon addition of excess Cu^{2+}.

*X-ray Crystallographic Structure Determination of Adduct **II** in Y369F.* In Figure 7A, the active site of adduct **II** in Y369F from a crystal structure solved at 2.3 Å resolution is shown. Adduct **II** is shown to be the copper-coordinated form of TPQ−2HP, which exists as the fully deprotonated azo tautomer where the charge is neutralized by Cu^{2+}, in good agreement with the structure of **3**. The O4 of TPQ−2HP is 2.9 Å from the Cu^{2+} and is within hydrogen-bonding distance of a water molecule (W2) lying 3.3 Å from the Cu^{2+}. The

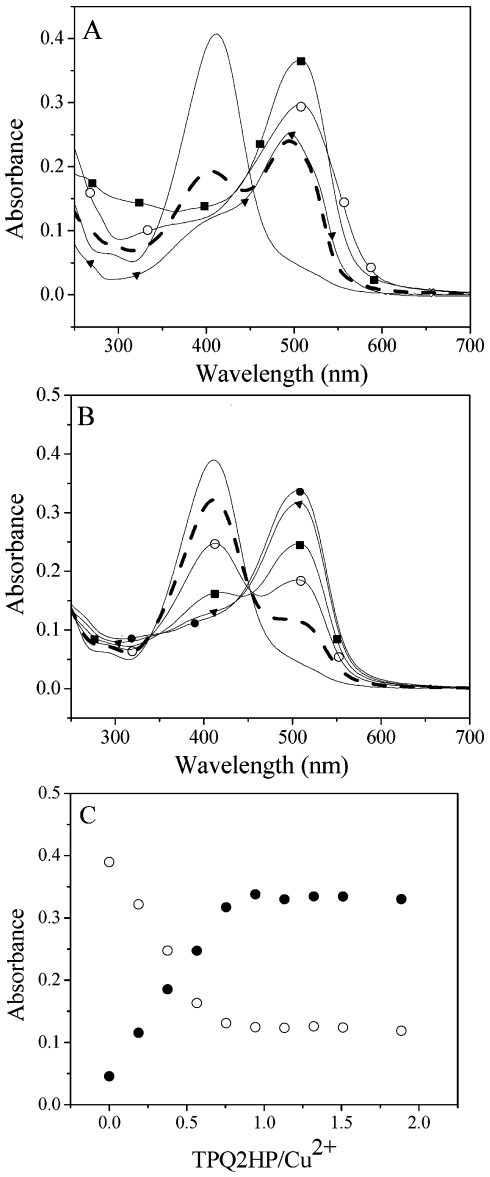

FIGURE 6: (A) Effect of divalent cations on the UV−vis spectrum of **2** at 25 °C, pH 7.3. Key: (—) **2**, (■) **2** + Cu^{2+}, (○) **2** + Co^{2+}, (▲) **2** + Ni^{2+}, (- - -) **2** + Zn^{2+}. (B) Spectra showing the titration of **2** with Cu^{2+}. Key: (—) **2**, (- - -) **2** + 0.2 molar equiv of Cu^{2+}, (○) **2** + 0.4 molar equiv of Cu^{2+}, (■) **2** + 0.6 molar equiv of Cu^{2+}, (▲) **2** + 0.8 molar equiv of Cu^{2+}, and (●) **2** + 1 molar equiv of Cu^{2+}. (C) Plot showing A_{414} (○) decrease and A_{506} (●) increase as a function of Cu^{2+} addition to **2**.

O2 of TPQ−2HP interacts via another water molecule, W4, with a carboxylate oxygen of D383 as seen in the resting form of Y369F. In comparison to the structure of adduct **I** in WT-ECAO (Figure 2A), the orientation of the pyridine ring with respect to the TPQ ring is altered, and the two rings are now coplanar, indicative of the azo tautomer. The pK_a of D383 in the resting form of Y369F is determined to be 6.5, ca. 0.8 pH unit elevated from that in the WT (*2*). Assuming the pK_as of D383 in the resting form and Y369F adduct **II** are not significantly perturbed under the crystallization conditions (pH 6.9−7.3), approximately 76% of D383 would then be in the deprotonated state. W4 (see Figure 1) could buffer the negative charge on D383 to reduce the repulsion with the anionic O2 of TPQ both in the resting form and in adduct **II** of Y369F.

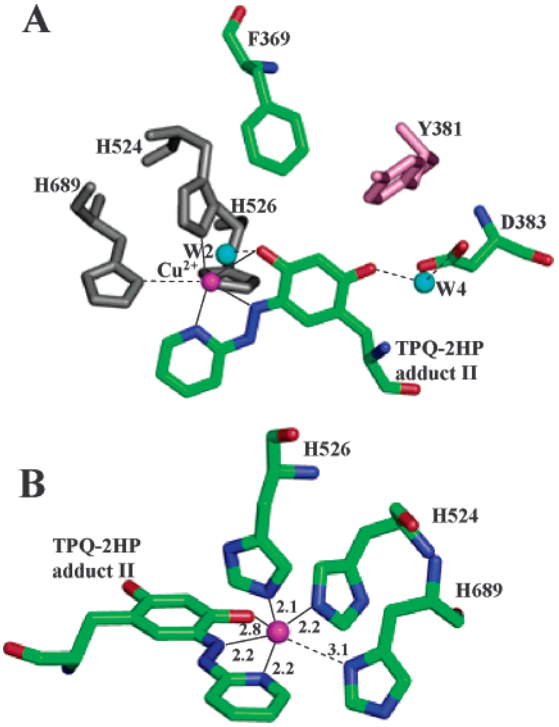

FIGURE 7: Active site structure of Y369F adduct **II** (A) and the copper site of Y369F adduct **II** (B) (magenta sphere, copper; blue spheres, water).

Copper coordination geometry of adduct **II** in Y369F is shown in more detail in Figure 7B. The active site Cu^{2+} in ECAO is five coordinate, where one of the His ligands (H689) and the two water ligands are displaced by TPQ−2HP to form a distorted square-pyramidal geometry. The coordination sphere of Cu^{2+} is known to be relatively labile (*10*), changing from five to four coordinate by losing one of the water ligands. Cu^{2+} is in a rough plane comprising N1 and N3 of the azo moiety and the nitrogens of H524 and H526. O4 of TPQ−2HP sits on the Jahn−Teller axis.

*X-ray Crystallographic Structure Determination of **3**.* To further characterize the complex formed between Cu^{2+} and **2**, [(phen)Cu^{II}(**2**)] (**3**) was isolated from a methanolic solution containing **2**, $CuCl_2$, and 1,10-phenanthroline in the presence of NaOMe, and its structure was determined by X-ray crystallography. There are four molecules of the copper complex in the unit cell of the primitive, monoclinic space group $P2_1/a$. Associated with each molecule of the copper complex are four waters of crystallization. These waters form hydrogen bonds to each other throughout the lattice and to the coordinated oxygen O4, the hydroxyl oxygen O2, and one of the azo nitrogens, N2, forming a three-dimensional hydrogen bond network. The water molecules are located in a channel which runs perpendicular to the *b*/*c* plane. The copper has a distorted five-coordinate square-pyramidal geometry and is bonded in a rough plane to O4, N1, and N3 of the azo moiety and one of the nitrogens, N4, of the 1,10-phenanthroline ligand (Figure 8). The distortion from a square-pyramidal geometry is due to the bite angle of the 1,10-phenanthroline ligand. The bond from Cu^{2+} to N5 is significantly longer (2.23 Å) than to the other phenanthroline nitrogen, N4 (2.03 Å), due to Jahn−Teller effects. The planes of the phenanthroline and the 2HP ring systems are almost orthogonal to each other. Compound **3** crystallized with a

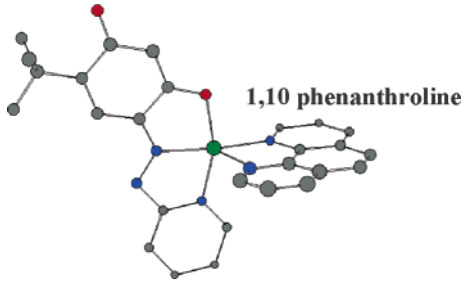

FIGURE 8: Crystal structure of **3** (gray spheres, carbon; red spheres, oxygen; blue spheres, nitrogen; green sphere, copper).

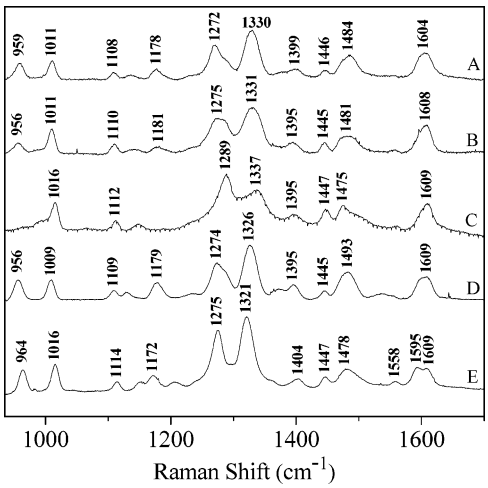

FIGURE 9: Resonance Raman spectra of adduct **II** in (A) WT-ECAO, (B) D383N, (C) D383E, (D) Y369F, and (E) model compound **2** with Cu^{2+} (200 μM in 0.1 M potassium phosphate, pH 7.2). Protein concentrations ranged from 48 to 91 μM in 0.1 M potassium phosphate, pH 7.2. Data were collected using an excitation wavelength at 514.5 nm.

Scheme 3: Resonance Structures of **3**

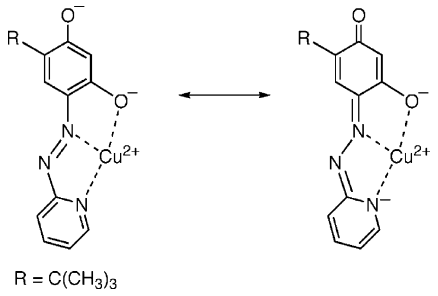

net neutral charge, so that the two hydroxyl groups of **2** are deprotonated in order to cancel the +2 charge on Cu. This explains the analogous effect of the divalent cations to deprotonation on the UV−vis spectrum of **2** (see above). The low pK_a of the 2-hydroxyl group of the TPQ−2HP ligand in **3** suggests that it exists as a resonance hybrid where the negative charge can be localized on the nitrogen coordinated directly to Cu^{2+} (Scheme 3).

*Resonance Raman Spectroscopy of **2** with MCl_2 (M = Cu^{2+} or Co^{2+}), **3**, and Adduct **II***. Figure 9 compares the rR spectra of adduct **II** in WT, D383N, D383E, Y369F, and **2** with $CuCl_2$. All spectra shown in Figure 9 are closely similar, suggesting that the mutation of D383 and Y369 does not affect the electronic nature of TPQ−2HP in adduct **II**. These results contrast with the clear influence of mutations on these residues seen on the UV−vis and rR spectroscopic properties of adduct **I** [see preceding paper (*26*)]. Figure 10 compares

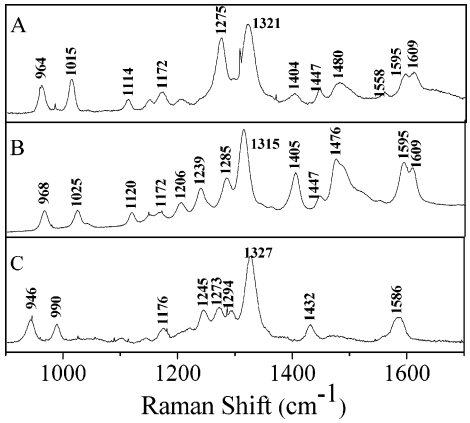

FIGURE 10: Resonance Raman spectra of **2** (200 μM) after the addition of (A) $CuCl_2$, (B) $CoCl_2$, and (C) NaOH. Metals were added to **2** in a 1:1 ratio. At high pH, 10 μL of **2** (200 μM) was added to 100 μL of 1 M NaOH to give a final pH of ~11. Data were collected at 514.5 nm excitation.

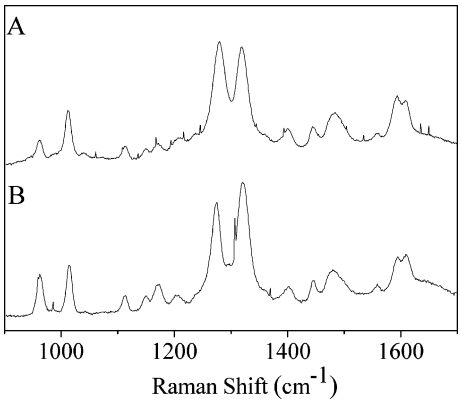

FIGURE 11: Resonance Raman spectra of **3** (A) and **2** with Cu^{2+} (B) prepared in 0.1 M potassium phosphate, pH 7.2. Data were collected using a 514.5 nm excitation wavelength and 40 mW power.

the rR spectra of the model compound **2** after the addition of (A) $CuCl_2$, (B) $CoCl_2$, and (C) NaOH. Each of those conditions caused the sample of **2** to turn pink, characteristic of adduct **II** formation. The rR spectrum of **2** after the addition of $CoCl_2$ (B) shows some peak assignments similar to that of **2** with $CuCl_2$ (A) specifically in the region from ~1400 to 1600 cm^{-1}. However, dramatic changes in peak intensity and frequencies occur in the region between 1120 and 1320 cm^{-1}, suggesting that the coordination environments of the TPQ−2HP complexes of Cu^{2+} and Co^{2+} are somewhat different. This conclusion is supported by the observation that the 1120−1320 cm^{-1} region is substantially different in the rR spectrum of **2** at high pH in the absence of a metal ion (Figure 10C). Indeed, the rR spectra of **2** with $CuCl_2$ (Figures 9E and 10A) and the species formed at high pH (Figure 10C) have practically no features in common, suggesting that metal ion coordination is required for adduct **II** formation. Collectively, the rR spectra in Figures 9 and 10 establish that adduct **II** is a Cu^{2+} complex. Figure 11 compares the rR spectra of model compound **3** and model compound **2** with $CuCl_2$ where the former contains 1,10-phenanthroline which is absent in the latter. The spectra are nearly superimposable, indicating that the electronic transitions and principal vibrational modes of both models are dominated by the TPQ−2HP−Cu^{2+} unit and are insensitive to the nature of the other Cu^{2+} ligands.

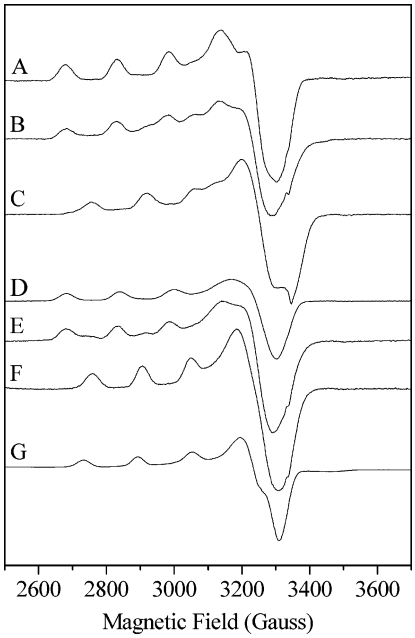

FIGURE 12: EPR spectra at 77 K of (A) WT-ECAO, (B) WT adduct **I** (C), WT adduct **II** (D), Y369F (E), Y369F adduct **I** (F), Y369F adduct **II**, and (G) **3**. Conditions: frequency modulation, 9.31 GHz; modulation amplitude, 12 G; microwave power, 2.00 mW.

Table 1: EPR Simulation Parameters for the Resting Form of WT, Y369F-ECAO, and Their 2-HP Adducts along with **3**

	$g_{\|\|}$	$A_{\|\|}$ (MHz)	$g_{\perp}$	coordination[a]
WT	2.292	492	2.0574	3N, 2O
WT adduct **I**	2.294	480	2.0590	3N, 2O
WT adduct **II**	2.230	447	2.0400	
Y369F	2.280	510	2.0500	3N, 2O
Y369F adduct **I**	2.290	488	2.0574	
Y369F adduct **II**	2.237	452	2.0500	4N, 1O
3	2.234	524	2.0580	4N, 1O

[a] From the crystal structure.

*EPR of WT-ECAO and Y369F Adducts **I** and **II***. EPR spectra of the resting, adduct **I**, and adduct **II** forms of WT-ECAO along with the EPR spectrum of **3** are shown in Figure 12. The spectra were simulated assuming axial *g*-tensors and corresponding hyperfine tensors (Table 1). The *g*-value pattern, $g_{\|} > g_{\perp} > 2.0$, of the resting form of WT and Y369F-ECAO is indicative of a $d_{x^2-y^2}$ ground state, consistent with the square-pyramidal geometry observed in the crystal structures of those forms. The values are comparable with those of other amine oxidases (*23*). Furthermore, the simulated $g_{\|}$ and $A_{\|}$ values support the mixed N,O copper ligation (*24*) as observed in the crystal structures of WT-ECAO, WT-ECAO adduct **I**, Y369F, and Y369F adduct **II**. The *g*-values and $A_{\|}$ for adduct **I** in WT-ECAO and Y369F (Figure 12B,E) are comparable to the resting forms, indicating that the copper ion has not been significantly perturbed. Similar behavior is observed when derivatizing amine oxidase from bovine serum with phenylhydrazine (*25*). The EPR spectra of adduct **II** in WT-ECAO and Y369F are characterized by reduced $g_{\|}$ and hyperfine coupling constants in comparison with the resting forms or adduct **I** spectra. Comparison of Peisach and Blumberg diagrams (*24*) supports the interpretation that changes in the *g*-values and hyperfine coupling constants reflect a change in equatorial coordination geometry from 3N, 1O to 4N. Note that the EPR spectrum of the model compound **3** does not exhibit reduced $A_{\|}$ compared to Y369F adduct **II**, probably as a result of the different geometry and bond lengths in the model compound. In **3**, the copper ion has a distorted five-coordinate square-pyramidal geometry (due to the bite angle of the phen ligand), and the Cu−N5 bond is significantly longer (2.23 Å) than the other phen N ligand (2.03 Å).

DISCUSSION

The species formed by alkaline treatment of WT-ECAO adduct **I** displays a UV−vis spectrum very similar to that of adduct **II** at pH 7 and compound **2** at pH 14 (where **2** is fully deprotonated), which might suggest that adduct **II** is structurally related to the fully deprotonated form of **2**. However, adduct **I** in the enzyme is a monoanion at neutral pH (Scheme 4), raising the question as to how the second deprotonation can be induced by thermal incubation at 60 °C. Further, it is not immediately obvious why such a deprotonation should be time dependent and irreversible.

To explain the nature of the thermally induced adduct **II** formation, we proposed that specific interactions between the TPQ−2HP moiety and D383, Y369, and Y381 in adduct **I** [see preceding paper (*26*)] are disrupted, thereby increasing the mobility of the complex. This is consistent with the pH-dependent nature of adduct **I** to adduct **II** conversion. The increased mobility could allow for new interactions with other active site residues to facilitate the full deprotonation of TPQ−2HP. An alternate proposal is that, at 60 °C, the TPQ−2HP moiety has a sufficient range of motion to directly move on to the active site Cu^{2+}, where Cu^{2+} can act as a Lewis acid to stabilize the dianionic form of TPQ−2HP. The first possibility was shown to be unlikely as the second pK_a of TPQ−2HP is >13 [see preceding paper (*26*)] and there are no active site residues sufficiently basic to facilitate this deprotonation. The second possibility is consistent with the X-ray crystallographic structures of WT adduct **I** and Y369F adduct **II** (Figure 13). Such an active site rearrangement for 2HP-inhibited ECAO is remarkable given the steric demands of the derivatized TPQ within a specific wedge-shaped cavity in the active site (*8*) (Figure 14). This wedge cavity was discovered by inspection of the van der Waals surfaces of active site residues such as V367, Y369, D383, N465, and A491, surrounding the TPQ cofactor in the crystal structure of WT-ECAO (*8*, *10*). This cavity is found in all four CAOs whose structures have been determined, and the residues forming the sides of the wedge, V367 and N465, are conserved in all four species. Formation of adduct **II** in WT-ECAO requires relatively severe conditions in order to break the H-bonding and hydrophobic interactions within the active site. This meant that there was no reasonable way of generating crystals of 2HP-derivatized WT-ECAO with a full complement of adduct **II**. An obvious way to break those hydrogen bonds under mild conditions is by site-directed mutagenesis. Y369F proved to be the appropriate system to generate adduct **II** in high yield at neutral pH without the need for thermal incubation at high temperature. Consequently, we were able to obtain a crystal structure of adduct **II** in Y369F-ECAO. The spectroscopic data, especially the rR and EPR spectra (Figures 9 and 12), unequivocally establish that adduct **II** in the WT-ECAO and in the Y369F variant are identical. Thus, the structure of the Cu^{2+}−TPQ−

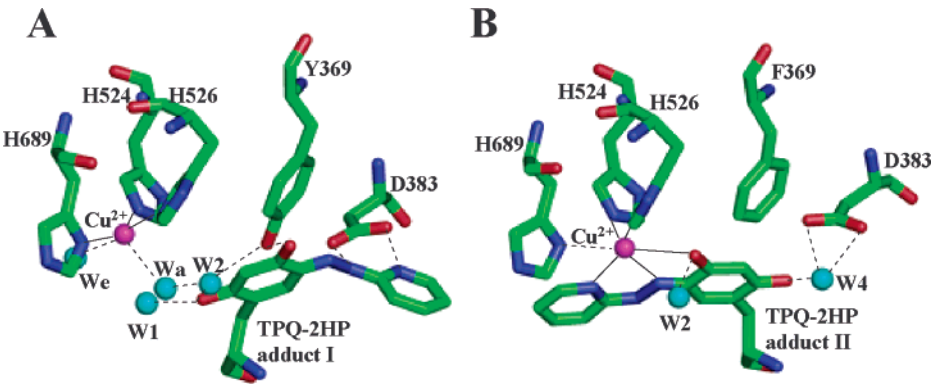

FIGURE 13: Crystal structures of WT-ECAO adduct **I** (A) and Y369F adduct **II** (B) (magenta sphere, copper; blue spheres, water).

Scheme 4: Hydrazone to Azo Conversion of Adduct **I**

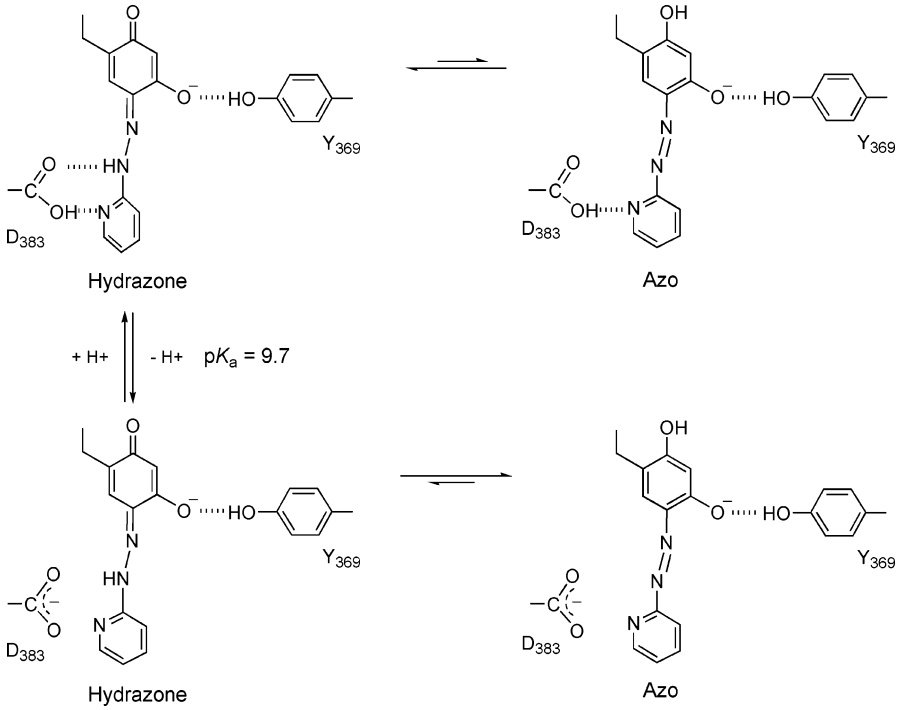

2HP complex shown in Figure 8 must also be the structure of adduct **II** in WT-ECAO.

Comparisons among the ECAO enzymes and the model compounds **2** and **3** provide additional confirmation of this key point. A simple reaction between **2** and Cu^{2+} produced a spectral change that matched that of the adduct **I** to adduct **II** conversion, strongly supporting the second proposal. In addition, we were able to obtain the crystal structure of a model compound, **3**, whose UV−vis and rR spectra showed an excellent match with those of adduct **II** and to those of the product of the reaction of **2** with Cu^{2+}. These results confirm that adduct **II** was indeed the Cu-coordinated form of TPQ−2HP.

The observation that adduct **II** is a copper-coordinated TPQ−2HP species is both unprecedented and surprising. To our knowledge, this is a unique rearrangement in the coordination chemistry of metalloenzymes and a novel mechanism for irreversible inactivation of an enzyme. To accommodate the large movement of TPQ−2HP in the active site, there must be a series of concerted movements of the active site residues (Figure 14). There appears to be only one direction in which TPQ−2HP can relocate from the wedge-shaped cavity that is evident in the crystal structure of WT-ECAO (*5*, *8*). There is a "wall" comprised of the peptide backbone at one face of TPQ such that movement of the side chains along the other face of TPQ, where there is an opening in the wedge, is likely to be the thermally accessible path for rearrangement. Further inspection of the active site structure of WT and Y369F shows that the hydroxyl group of Y369 acts as a "bar" across the open side of the wedge. Heating the solution to 60 °C or denaturation with 8 M urea will help the wedge to "breathe" so that TPQ−2HP can swing out from the cavity through the opening in the wedge in WT-ECAO. Alternatively, breaking the interaction between O4 of TPQ and the hydroxyl group of Tyr369 by site-directed mutagenesis (Y369F) also provides adduct **I** with enough range of motion to swing out of the wedge (Figure 14B). This shows that TPQ is held in position by a combination of the wedge and by the hydrogen-bonding interaction involving Tyr369. Disrupting either of these interactions increases the degree of mobility of TPQ−2HP within the active site.

The flexibility of TPQ has been highlighted in the crystal structures of the underivatized resting forms of WT-ECAO

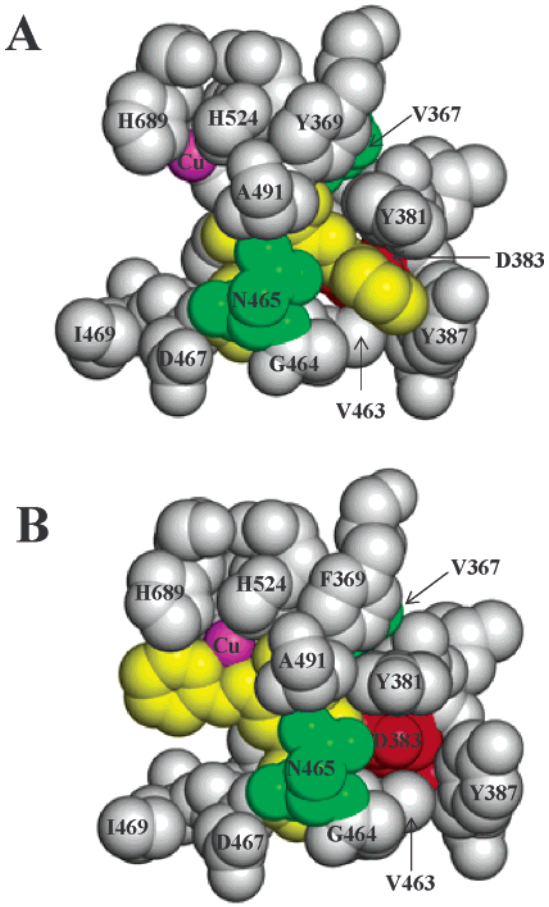

FIGURE 14: (A) Side view of a space-filling model showing the specific wedge-shaped cavity where the TPQ−2HP (yellow) is located in ECAO adduct **I**. Important active site residues surrounding TPQ are labeled. (B) Same view as in (A) depicting the dramatic movement of the TPQ−2HP (yellow) to the on-copper conformation in Y369F adduct **II**.

(*8*), D383A (*8*), and Y369F (*2*) where the cofactor can adopt a variety of conformations. The precise orientation of TPQ in these samples varies depending on the mutant being studied and on the conditions under which the crystals were obtained. It has been observed in active site mutants of HPAO, such as E406N (*14*), N404A (*15*), Y305A (*9*), and D319E (*16*), that the TPQ cofactor and TPQ-derived reaction intermediates observed under turnover conditions appear to be able to adopt catalytically compromised conformations. These effects are pH dependent and are manifested in a significant decrease in the enzyme activity. The present results on the formation and characterization of adduct **II** demonstrate that the TPQ−2HP moiety, *which has the similar size to the substrate and product Schiff base intermediates in the catalytic cycle*, can rearrange and coordinate the active site Cu^{2+} when the hydrogen-bonding interactions which keep the TPQ cofactor in the correct orientation are disrupted. The strongly favorable chelate effect of the TPQ−2HP adduct enabled us to trap the Cu^{2+}-coordinated form, which was stable enough to pursue full spectroscopic and structural characterization.

The pH dependence of the rate of adduct **II** formation in Y369F supports the assignment in this mutant of the pK_a at ~9.7 to D383 where the deprotonation will shift the hydrazone−azo equilibrium to the azo tautomer in adduct **I**. We have proposed in the preceding paper (*26*) that the short hydrogen-bonding interaction between D383 and the pyridine nitrogen of the 2HP moiety observed in the crystal structure of WT-ECAO adduct **I** is the reason for this high pK_a value of D383. It might seem more likely that this pK_a of 9.7 is due to deprotonation of the hydroxyl group of Y369 since it is well above the pK_a of Asp383 in the resting form (5.7). However, this latter possibility is considered unlikely since (i) adduct **II** formation in Y369F is faster at pH 9 when compared to pH 7 and (ii) the pH effect on the adduct **II** formation is absent in D383E and D383N; it is not possible to induce adduct **II** formation in these active site base mutants below pH 10, suggesting that the hydroxyl group of Y369 remains protonated.

CONCLUSIONS

We have unambiguously shown that the adduct **II** form of 2HP-inhibited ECAO is a novel Cu^{2+}-coordinated form of the complex where TPQ−2HP exists as the fully deprotonated azo tautomer. The hydrogen-bonding interactions within the active site of WT-ECAO at pH 7, 25 °C, are sufficient to suppress the conformational flexibility of TPQ−2HP and can stabilize the hydrazone tautomer. In Y369F, where the hydrogen bond between the hydroxyl group of Y369 and O4 of TPQ is eliminated, TPQ−2HP has increased mobility and is able to undergo facile migration to the Cu^{2+} site. We were able to trap the Cu^{2+}-coordinated conformation due to the excellent chelating properties of TPQ−2HP. The present study strongly supports the proposal that the essential role of Y369 is to keep TPQ and the reaction intermediates in an optimal conformation during the catalytic cycle (*2*, *7*−*10*).

ACKNOWLEDGMENT

M.M. thanks Judith Klinman for providing support for M.M. to work on this project, Allen G. Oliver (X-ray Crystallographic Facility at UCB) for structural determination of **3**, and Julian Limburg for critical reading of the manuscript and valuable discussions.

SUPPORTING INFORMATION AVAILABLE

Experimental details for the X-ray structure determination of **3**. This material is available free of charge via the Internet at http://pubs.acs.org.

REFERENCES

1. Tipping, A. J., and McPherson, M. J. (1995) Cloning and molecular analysis of the pea seedling copper amine oxidase, *J. Biol. Chem. 270*, 16939−16946.
2. Murray, J. M., Kurtis, C. R., Tambyrajah, W., Saysell, C. G., Wilmot, C. M., Parsons, M. R., Phillips, S. E. V., Knowles, P. F., and McPherson, M. J. (2001) Conserved tyrosine-369 in the active site of *Escherichia coli* copper amine oxidase is not essential, *Biochemistry 40*, 12808−12818.
3. Li, R. B., Klinman, J. P., and Mathews, F. S. (1998) Copper amine oxidase from *Hansenula polymorpha*: The crystal structure determined at 2.4 Å resolution reveals the active conformation, *Structure 6*, 293−307.
4. Kishishita, S., Okajima, T., Kim, M., Yamaguchi, H., Hirota, S., Suzuki, S., Kuroda, S., Tanizawa, K., and Mure, M. (2003) Role of copper ion in bacterial copper amine oxidase: Spectroscopic and crystallographic studies of metal-substituted enzymes, *J. Am. Chem. Soc. 125*, 1041−1055.
5. Parsons, M. R., Convery, M. A., Wilmot, C. M., Yadav, K. D. S., Blakeley, V., Corner, A. S., Phillips, S. E. V., McPherson, M. J., and Knowles, P. F. (1995) Crystal structure of a quinoenzyme:

Copper amine oxidase of *Escherichia coli* at 2 Å resolution, *Structure 3*, 1171−1184.
6. Wilce, M. C. J., Dooley, D. M., Freeman, H. C., Guss, J. M., Matsunami, H., McIntire, W. S., Ruggiero, C. E., Tanizawa, K., and Yamaguchi, H. (1997) Crystal structures of the copper-containing amine oxidase from *Arthrobacter globiformis* in the holo and apo forms: Implications for the biogenesis of topaquinone, *Biochemistry 36*, 16116−16133.
7. Wilmot, C. M., Hajdu, J., McPherson, M. J., Knowles, P. F., and Phillips, S. E. V. (1999) Visualization of dioxygen bound to copper during enzyme catalysis, *Science 286*, 1724−1728.
8. Murray, J. M., Saysell, C. G., Wilmot, C. M., Tambyrajah, W. S., Jaeger, J., Knowles, P. F., Phillips, S. E. V., and McPherson, M. J. (1999) The active site base controls cofactor reactivity in *Escherichia coli* amine oxidase: X-ray crystallographic studies with mutational variants, *Biochemistry 38*, 8217−8227.
9. Hevel, J. M., Mills, S. A., and Klinman, J. P. (1999) Mutation of a strictly conserved, active-site residue alters substrate specificity and cofactor biogenesis in a copper amine oxidase, *Biochemistry 38*, 3683−3693.
10. Mure, M. (2004) Tyrosine-derived quinone cofactors, *Acc. Chem. Res. 37*, 131−139.
11. Wilmot, C. M., Murray, J. M., Alton, G., Parsons, M. R., Convery, M. A., Blakeley, V., Corner, A. S., Palcic, M. M., Knowles, P. F., McPherson, M. J., and Phillips, S. E. V. (1997) Catalytic mechanism of the quinoenzyme amine oxidase from *Escherichia coli*: Exploring the reductive half-reaction, *Biochemistry 36*, 1608−1620.
12. Su, Q. J., and Klinman, J. P. (1998) Probing the mechanism of proton coupled electron transfer to dioxygen: The oxidative half-reaction of bovine serum amine oxidase, *Biochemistry 37*, 12513−12525.
13. Saysell, C. G., Murray, J. M., Wilmot, C. M., Brown, D. E., Dooley, D. M., Phillips, S. E. V., McPherson, M. J., and Knowles, P. F. (2000) Investigation into the mechanism of lamda max shifts and their dependence on pH for the 2-hydrazinopyridine derivatives of two copper amine oxidases, *J. Mol. Catal. B 8*, 17−25.
14. Cai, D. Y., Dove, J., Nakamura, N., Sanders-Loehr, J., and Klinman, J. P. (1997) Mechanism-based inactivation of a yeast methylamine oxidase mutant: Implications for the functional role of the consensus sequence surrounding topaquinone, *Biochemistry 36*, 11472−11478.
15. Schwartz, B., Green, E. L., Sanders-Loehr, J., and Klinman, J. P. (1998) Relationship between conserved consensus site residues and the productive conformation for the TPQ cofactor in a copper-containing amine oxidase from yeast, *Biochemistry 37*, 16591−16600.
16. Plastino, J., Green, E. L., Sanders-Loehr, J., and Klinman, J. P. (1999) An unexpected role for the active site base in cofactor orientation and flexibility in the copper amine oxidase from *Hansenula polymorpha*, *Biochemistry 38*, 8204−8216.
17. Bailey, S. (1994) The CCP4 Suite: Programs for Protein Crystallography, *Acta Crystallogr., Sect. D: Biol. Crystallogr. 50*, 760−763.
18. Otwinowski, Z., and Minor, W. (1997), *Methods Enzymol. 267*, 307−326.
19. SMART: Area detector software package (1995) Bruker Analytical X-ray Systems, Inc., Madison, WI.
20. Altomare, A., Burla, M. C., Camalli, M., Cascarano, G., Giacovazzo, C., Guagliardi, A., Moliterni, A. G. G., Polidori, G., and Spagna, R. (1999) *SIR97:* A new tool for crystal structure determination and refinement, *J. Appl. Crystallogr. 32*, 115−119.
21. Beurskens, P. T., Admiraal, G., Beurskens, G., Bosman, W. P., de Gelder, R., Israel, R., and Smits, J. M. M. (1994) The DIRDIF-94 program system, Technical Report of the Crystallography Laboratory, University of Nijmegen, The Netherlands.
22. Janes, S. M., Palcic, M. M., Scaman, C. H., Smith, A. J., Brown, D. E., Dooley, D. M., Mure, M., and Klinman, J. P. (1992) Identification of topaquinone and its consensus sequence in copper amine oxidases, *Biochemistry 31*, 12147−12154.
23. McIntire, W. S., and Hartmann, C. (1993) Copper-containing amine oxidases in *Principles and Applications of Quinoproteins* (Davidson, V. L., Ed.) pp 97−171, Marcel Dekker, New York.
24. Peisach, J., and Blumberg, W. E. (1974) Structural implications derived from the analysis of electron paramagnetic resonance spectra of natural and artificial copper proteins, *Arch. Biochem. Biophys. 165*, 691−708.
25. Suzuki, S., Sakurai, T., Nakahara, A., Manabe, T., and Okuyama, T. (1983) Effect of metal substitution on the chromophore of bovine serum amine oxidase, *Biochemistry 22*, 1630−1635.
26. Mure, M., Brown, D. E., Saysell, C., Rogers, M. S., Wilmot, C. M., Kurtis, C. R., McPherson, M. J., Phillips, S. E. V., Knowles, P. F., and Dooley, D. M. (2005) *Biochemistry 44*, 1568−1582.

BI0479860